Microsphere-Coupled Scanning Laser Confocal Nanoscope for Sub-Diffraction-Limited Imaging at 25 nm Lateral Resolution in the Visible Spectrum

Yinzhou Yan,[†,‡] Lin Li,[†,*] Chao Feng,[‡] Wei Guo,[†] Seoungjun Lee,[†] and Minghui Hong[§]

[†]Laser Processing Research Centre, School of Mechanical, Aerospace and Civil Engineering, The University of Manchester, Manchester M13 9PL, U.K., [‡]Institute of Laser Engineering, Beijing University of Technology, Beijing 100124, People's Republic of China, and [§]Department of Electrical and Computing Engineering, National University of Singapore, Singapore 117583, Singapore

ABSTRACT We report a direct optical super-resolution imaging approach with 25 nm ($\sim\lambda/17$) lateral resolution under 408 nm wavelength illumination by combining fused silica and polystyrene microspheres with a conventional scanning laser confocal microscope (SLCM). The microsphere deposited on the target surface generates a nanoscale central lobe illuminating a sub-diffraction-limited cross-section located on the target surface. The SLCM confocal pinhole isolates the reflected light from the near-field subdiffractive cross-section and suppresses the noises from the side lobe and the far-field paraxial focal point. The structural detail of the subdiffractive cross-section is therefore captured, and the 2D target surface near the bottom of microspheres can be imaged by intensity-based point scanning.

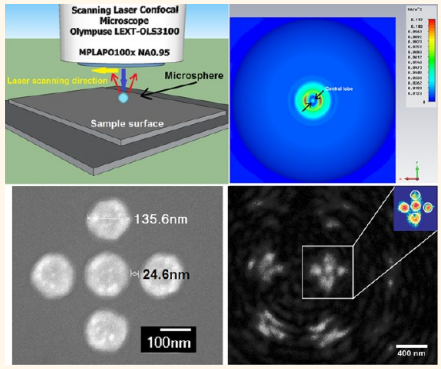

KEYWORDS: super-resolution · imaging · microsphere · scanning laser confocal microscope · nanoscope · diffraction limit

Abbe's diffraction limit is generally recognized as the ultimate barrier in optical imaging by far-field lens-based optical microscopes. Numerous efforts have been attempted to overcome the classical diffraction limit ($\sim\lambda/2$, where λ is the light wavelength) and achieve super-resolution imaging in the past few decades. Recovery of nonpropagating evanescent waves that contain diffraction-free and fine details of the electromagnetic (EM) waves in the near-field (within the distance of the optical wavelength) is a major approach achieving sub-diffraction-limited imaging. Several direct optical imaging (*i.e.*, nonflorescence) techniques have been reported including scanning near-field optical microscopy (SNOM),[1−4] metamaterial superlens,[5−10] solid immersion lens (SIL),[11,12] *et al.* The far-field super-resolution imaging has also been demonstrated by a superoscillatory lens (SOL), which focused sub-diffraction-limited hot spots at a typical distance of 10 μm from a nanostructured binary mask.[13−15] The imaging resolution *via* the superoscillatory lens was around $\lambda/6$ (105 nm).[16]

Compared with the above techniques, nanoscale solid immersion lenses,[17,18] surface plasmon polariton (SPP)-enhanced microdroplets,[19,20] and microfiber[21] coupling with a conventional optical microscope provide alternative ways to achieve optical super-resolution imaging. The resolutions *via* these superlenses were 126 nm ($\lambda/4$), 60 nm ($\lambda/8$), and 70 nm ($\lambda/8$), respectively. In 2011, a white-light optical microscope (WM) coupled with 2−9 μm fused silica microspheres (refractive index $n = 1.46$) in air was first demonstrated, where the achieved imaging resolution was ~50 nm ($\lambda/8$).[22] The mechanism of super-resolution imaging

* Address correspondence to Lin.li@manchester.ac.uk.

Received for review December 2, 2013 and accepted January 23, 2014.

Published online January 28, 2014
10.1021/nn406201q

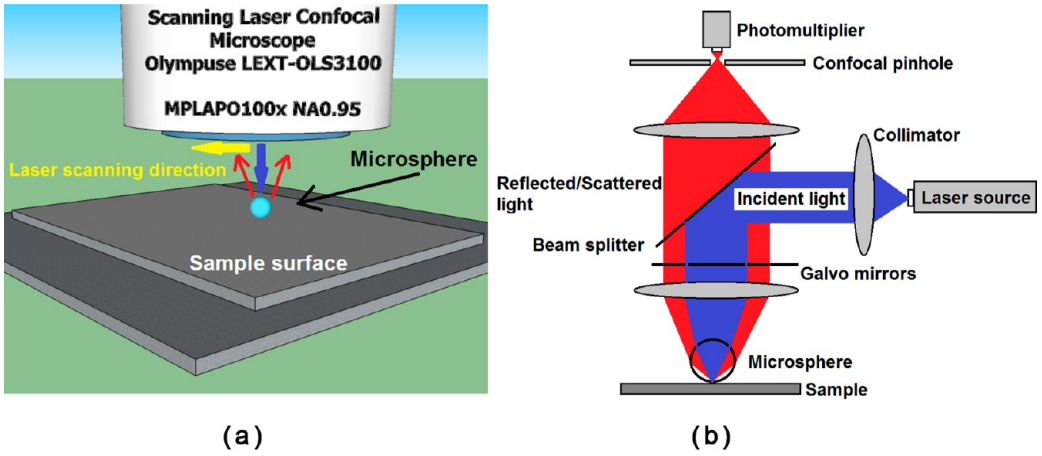

Figure 1. Experimental setup of the microsphere-coupled SLCM (mSLCM) under the reflection illumination mode. (a) Schematic of the experimental configuration. (b) Optical path of the mSLCM.

was explained as "photonic nanojet"[23−27]-enhanced sub-diffraction-limited illumination and conversion of the near-field evanescent waves to magnified far-field propagating waves by the microspheres.[28] The subsequent studies further indicated that the low-index microspheres (n = 1.46) semi-immersed in liquid can reinforce the super-resolution strength,[29] and the high-index microspheres (n = 1.9−2.1) with larger diameters (50−220 μm) totally submerged by a liquid layer could achieve super-resolution imaging down to $\lambda/7$.[30] Li *et al*. demonstrated the super-resolution imaging of 75 nm viruses by submerged microsphere optical microscopy without the use of fluorescent labeling or staining.[28] The effect of the surrounding liquid for immersed microsphere optical nanoscopy has been studied by Lee *et al*., showing that water is most effective.[31] The microsphere magnifications have also been studied for various microsphere sizes and distances to the target surface. The 6 to 8 times magnification was achieved by polystyrene (PS) microspheres with larger diameters (30−100 μm) in air,[32] whereas the magnification of 5 μm diameter fused silica microspheres semi-immersed in ethanol was limited at 1.47 times.[33] However, the resolution by large-diameter microspheres cannot break the record of 50 nm. Furthermore, the super-resolution imaging mechanism of the microsphere-coupled white-light optical nanoscopes was investigated and argued in previous work.[22,29,33−36] For practical applications of microsphere nanoscopy, Krivitsky *et al*. first employed a fine glass micropipet to control a microsphere for moving and positioning.[37] Such a method provides a way to achieve a wide field of view (FOV) by multiple nanoimaging through a moving microsphere.

In this work, we present a new technique by combining microspheres with a scanning laser confocal microscope (SLCM) for super-resolution imaging. As opposed to the conventional wide-field optical microscopes used in previous studies, the SLCM employs a focused laser as the illuminating light. The laser spot scans the whole focusing plane, and the reflected light intensity is detected *via* a pinhole-coupled photomultiplier.[38] The major difference of the imaging process from wide-field optical microscopy is that the SLCM collects the light intensity point by point in scanning and joins the "point" light intensities together to create an image, *i.e*., a point scanning imaging technique, rather than directly projecting a wide-field image on a CCD detector, which is commonly used in wide-field optical microscopes. In this study, we utilized the unique imaging approach, achieving super-resolution imaging far beyond the diffraction limit by coupling an SLCM with microspheres. The super-resolution imaging mechanism of the microsphere-coupled SLCM (mSLCM) was investigated.

RESULTS

Figure 1 shows a schematic of the experimental configuration for microsphere nanoimaging. The microspheres employed in this work were fused silica (FS) microspheres (n = 1.47 at 408 nm wavelength) with diameters of 2.5, 5, and 7.5 μm, as well as 5 μm diameter PS microspheres (n = 1.62 at 408 nm wavelength). An anodic aluminum oxide (AAO) template with 25 nm hole diameters and 25 nm edge-to-edge separations was used as the calibration (Figure 2a), which were not gold-coated in order to avoid the potential effect of metallic properties (*e.g*., SPPs) on the visible spectrum. Ag nanowires (NWs) with a diameter of 40 ± 5 nm (Figure 3a) and WO_3 NWs with a diameter of 50 ± 5 nm (Figure 3b) were also employed to exhibit the capability of the mSLCM for arbitrary nanopattern imaging. Moreover, an array of gold quintuplet nanodots coated on a glass substrate as shown in Figure 4a was used to demonstrate the spatial resolution of an mSLCM for two individual objects with a separation of 25 nm.

AAO (25 nm) Template Imaging Experiments. The AAO template captured by a standard SLCM is shown in Figure 2b. The hole array cannot be resolved because the 25 nm ($\lambda/17$) structural feature is far beyond the SLCM maximum resolution (*i.e*., 120 nm). Figure 2c shows the super-resolution imaging using a 5 μm diameter FS

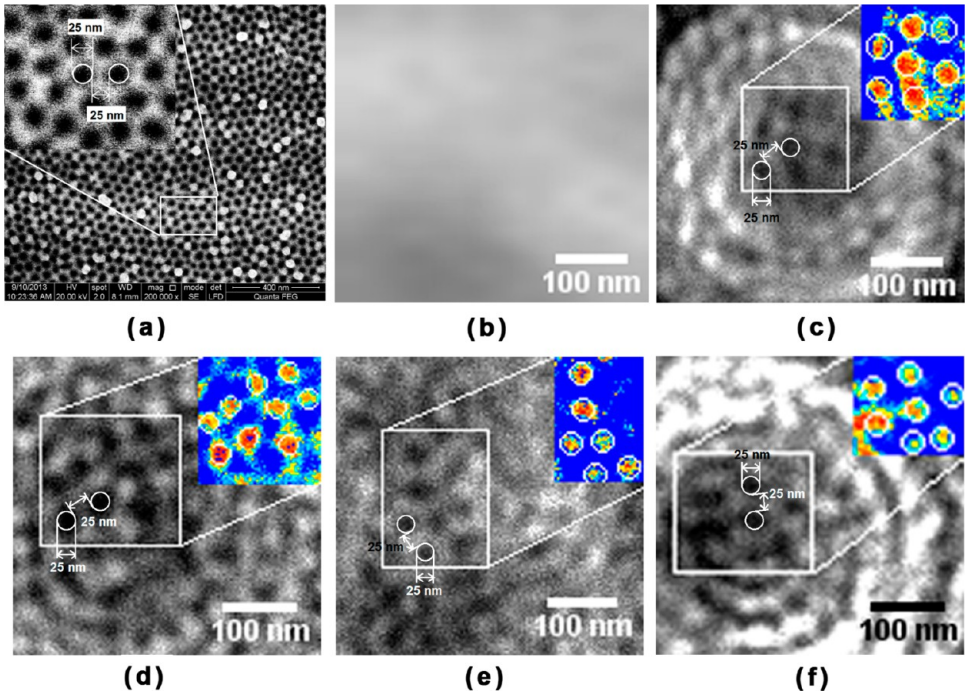

Figure 2. Micrographs of the 25 nm AAO template by (a) SEM, (b) standard SLCM, (c) 5 μm diameter FS mSLCM, (d) 2.5 μm diameter FS mSLCM, (e) 7.5 μm diameter FS mSLCM, and (f) 5 μm diameter PS mSLCM, where the insets are the corresponding pseudocolor images.

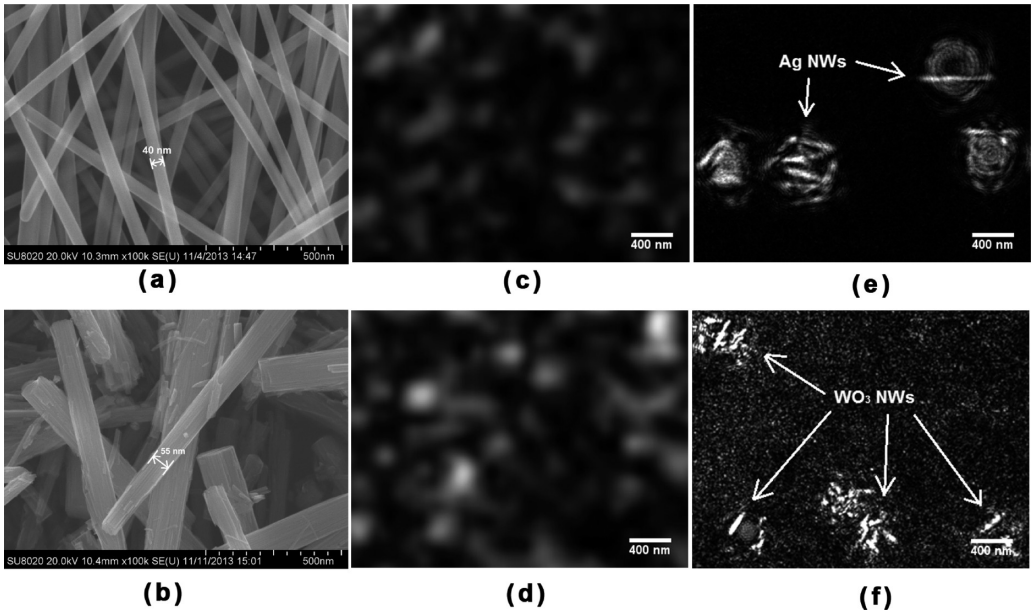

Figure 3. Images of 40 nm diameter Ag NWs and 50 nm diameter WO_3 NWs. The SEM images of (a) Ag NWs and (b) WO_3 NWs, the standard SLCM optical images of (c) Ag NWs and (d) WO_3 NWs, and the mSLCM optical super-resolution images of (e) Ag NWs and (f) WO_3 NWs by 5 μm diameter FS microspheres. The scale bars in (e) and (f) represent the lengths within the view fields by microspheres.

mSLCM. It can be clearly seen that the 25 nm holes and edge-to-edge separations are resolved. Such a 25 nm structural feature can also be observed using 2.5 μm diameter FS, 7.5 μm diameter FS, and 5 μm diameter PS microspheres, respectively, as shown in Figure 2d–f.

Nanowire Imaging Experiments. Ag NWs and WO_3 NWs were employed in this work to demonstrate the mSLCM imaging capability for arbitrary nanopatterns. Figure 3c and d shows that the 40 nm diameter ($\sim\lambda/10$) Ag NWs and 50 nm diameter ($\sim\lambda/8$) WO_3 NWs cannot be directly resolved *via* a standard SLCM. Under the 5 μm diameter FS mSLCM, the super-resolution Ag NWs and WO_3 NWs images can be observed as shown in Figure 3e and f, respectively. It can be clearly seen that the 40 nm diameter Ag NWs and 50 nm diameter WO_3 NWs are resolved. For nonmetallic WO_3 NWs, it should be

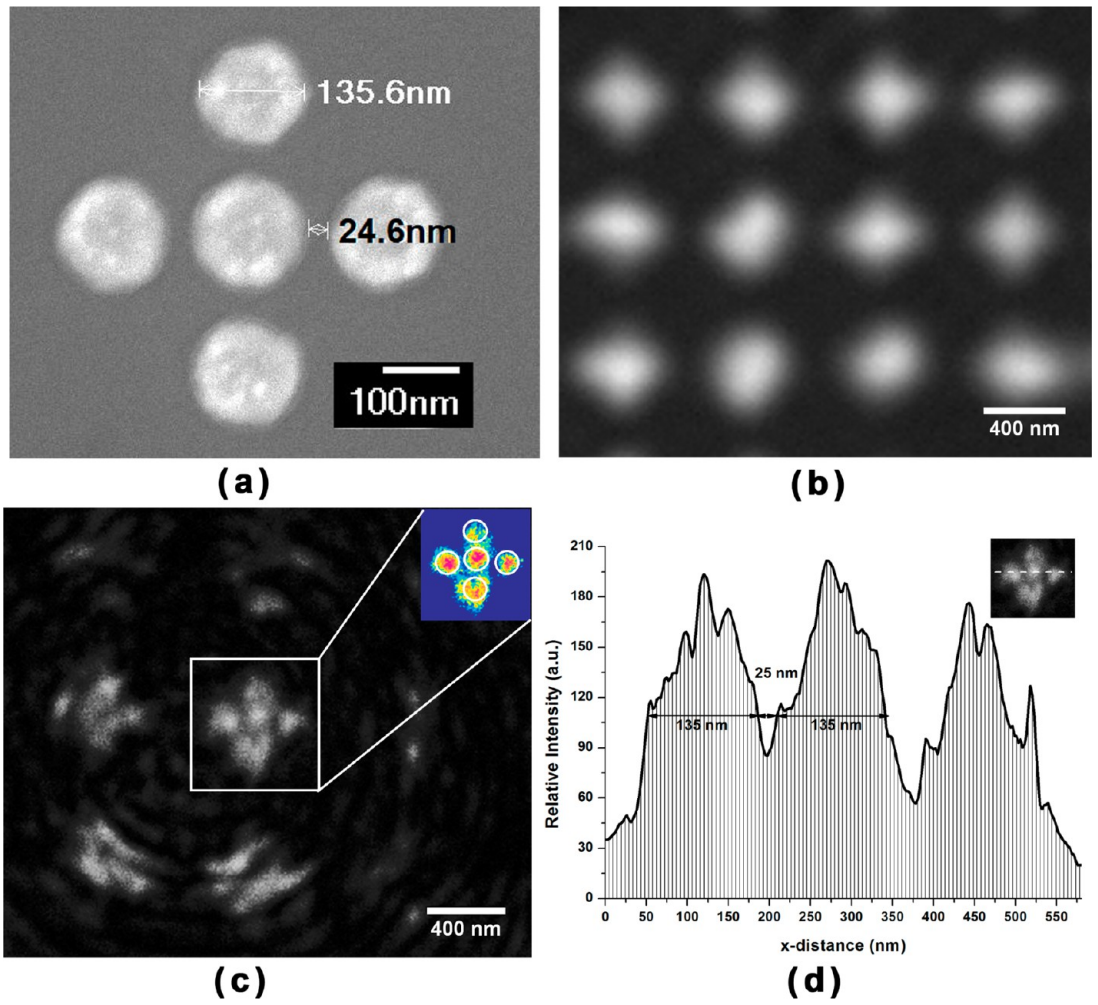

Figure 4. Images of gold quintuplet nanodots on a glass substrate by (a) SEM, (b) standard SLCM, and (c) 5 μm diameter FS mSLCM, where the inset is the corresponding pseudocolor image. The scale bar in (c) represents the length within the view field by the microsphere. (d) Intensity variation of (c) along the transverse cross-section.

noted that there is no effect of SPPs on super-resolution imaging *via* the dielectric microspheres.

Gold Quintuplet Nanodot Imaging Experiments. As can be seen in Figure 4b, the standard SLCM without microsphere coupling cannot distinguish the gold quintuplet nanodots with 25 nm (λ/17) separations of peripheral dots to the central one. However, the nanodots can be nearly resolved by the 5 μm diameter FS mSLCM, as shown in Figure 4c, in which the resolved nanodots set is close to the microsphere center (*i.e.*, contact of the microsphere and the substrate surface), whereas the rest is distorted and blurred. Figure 4d illustrates the intensity variation within the clear imaging region. It can be found that the 25 nm separations have lower imaging intensities than the nanodots. The experimental result indicates that the individual objects with subwavelength spatial separations can be nearly resolved by the mSLCM.

DISCUSSION

As opposed to the conventional wide-field optical microscope used in previous studies,[22,28−33] the SLCM employs a single laser beam to scan the focusing plane in a raster pattern. The laser beam is controlled by a pair of galvanometric mirrors and focused by objective lenses on the target surface (as Figure 1b). The intensity of the reflected light by the focused laser spot illumination is collected by the objective lenses and filtered by the confocal pinhole. The photons passing through the pinhole come exclusively from the focal point of the objective.[38] Compared with conventional optical microscopes, the SLCM imaging is based on reflecting light intensity from an illuminated point rather than a wide-field projection. The 2D image of SLCM comprises the intensity of each illuminated point on the target surface by scanning sampling. The focused laser spot size ($\sim\lambda$/2 in the far-field) determines the imaging resolution. Therefore, the maximum resolution of the standard SLCM ($\sim\lambda$/4) is half of the wide-field optical microscopy ($\sim\lambda$/2) limited by the Airy disk ($\sim\lambda$) point-spread function. If a microsphere can focus the laser beam into a sub-diffraction-limited illumination spot ($<\lambda$/2), a subwavelength reflecting cross-section on the target surface can be generated, as shown in Figure 5a. It should be noted that the reflected light is diffraction-limited, but its intensity is determined

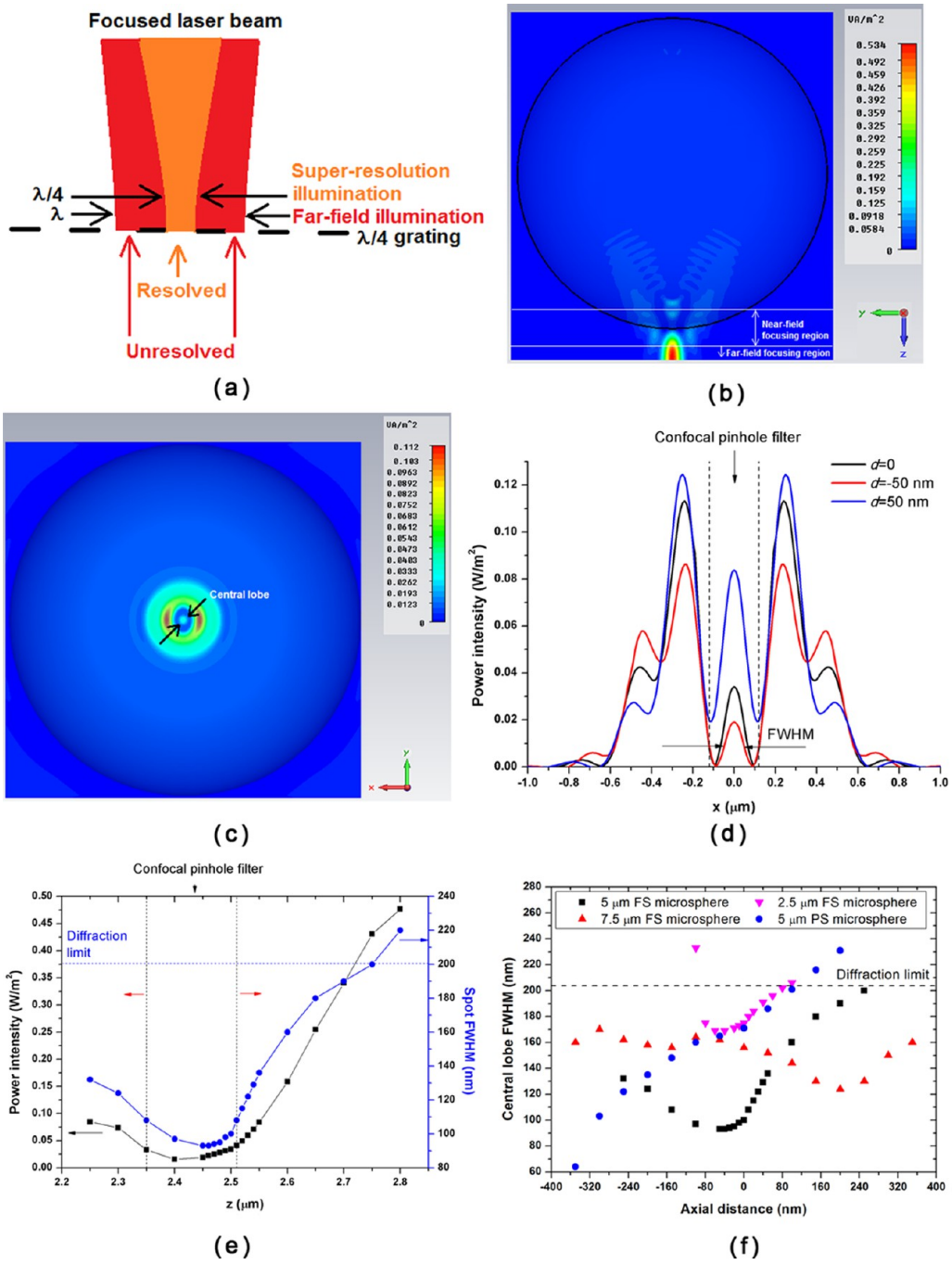

Figure 5. Numerical simulation of light focusing through a microsphere. (a) Schematic of far-field illumination and super-resolution illumination in SLCM imaging. (b) Front view and (c) top view of the EM distribution for a laser beam focused by a 5 μm diameter FS microsphere. (d) Intensity profile along the *x*-direction (*i.e.*, the lateral direction) in the plane away from the microsphere bottom with a distance, *d*, of −50, 0, and 50 nm. (e) Variation of power intensity and FWHM of the central lobe with a position (*z*) along the axial direction. (f) Variations of the central lobe FWHM on the target surface with the distance (*d*) from a perfect microsphere bottom for various microspheres.

by the structural feature of the sub-diffraction-limited reflection cross-section (*i.e.*, the reflectance of the local area), as in Figure 5a. Therefore, the imaging resolution depends on the reflecting cross-section size, *i.e.*, the focused laser spot size, rather than the Airy disk diameter. Then the 2D super-resolution image is obtained by collecting and joining all reflecting light intensities from the corresponding subwavelength reflecting cross-sections in the microsphere focusing plane by point scanning sampling.

In order to validate the above hypothesis, the process of illumination light focusing by a microsphere was simulated *via* finite difference in time domain (FDTD). Figure 5b and c demonstrate a typical intensity contour of a laser beam focused by a 5 μm diameter FS microsphere. It can be seen that a shiny nanoscale spot

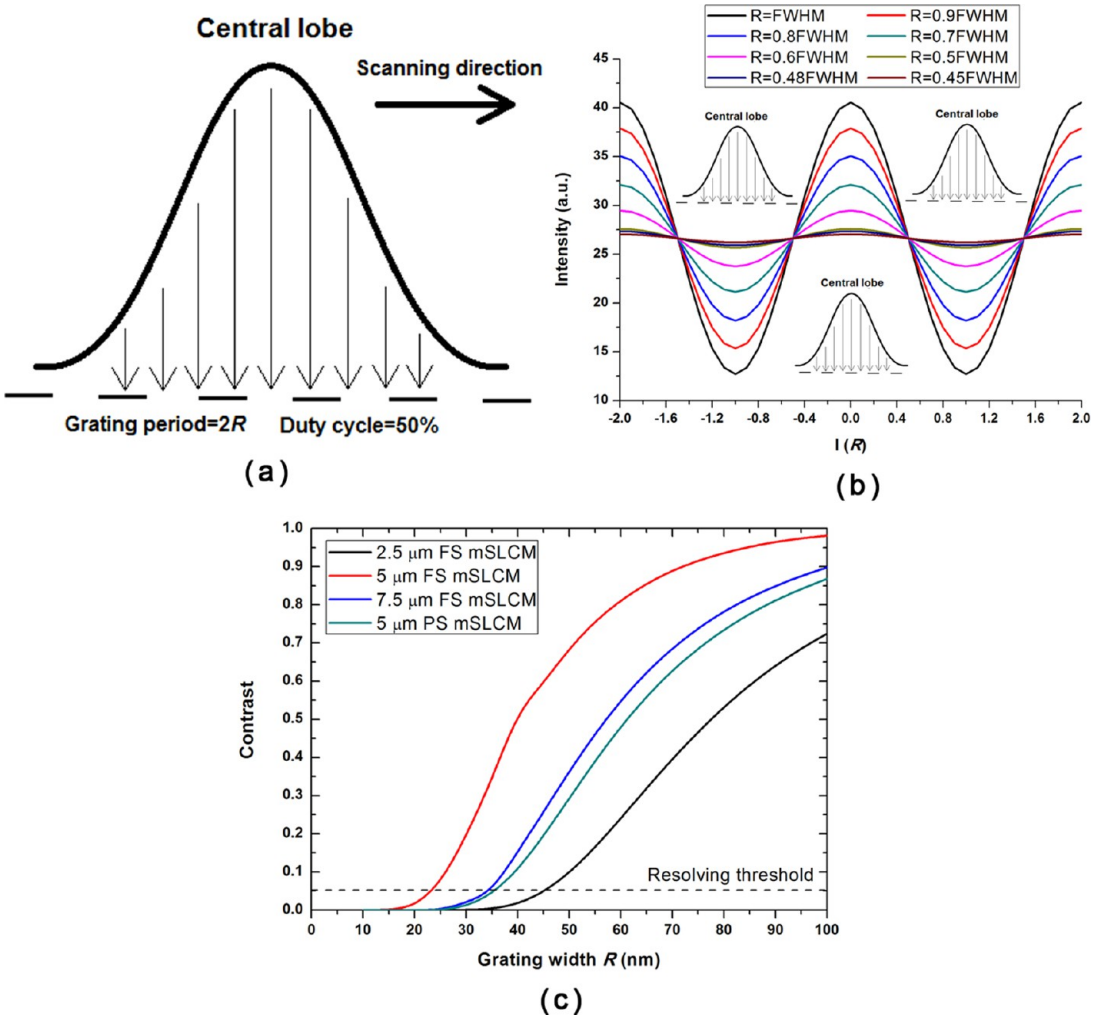

Figure 6. Reflected light intensity profile during the subdiffractive illumination spot scanning of a grating structure. (a) Schematic of a subdiffractive illumination spot scanning of a grating structure. (b) Light intensity profiles of various gratings imaged by subdiffractive illumination spot scanning. (c) Contrasts of super-resolution images for various microspheres and grating periods.

(central lobe) exists in the oscillatory field near the microsphere bottom. The full width at half-maximum (FWHM) is around 100 nm ($\lambda/4$) in air. It is much smaller than the diffraction limit (*i.e.*, 204 nm) at 408 nm wavelength. Compared with the previous studies using wide-field white-light microscopes,[22,32,33,36] the nanoscale spot here exists away from the far-field paraxial focusing region of the microsphere (Figure 5b). Moreover, as shown in Figure 5c, the transverse distribution of light intensity in the oscillatory field near the microsphere bottom is similar to the intensity profile *via* a superoscillatory lens.[14,16,39] This means that the microsphere is a natural superoscillatory lens in the near-field.

However, it can be seen in Figure 5d that the side lobe in the oscillatory field near the microsphere bottom contains the vast majority of the light energy. This would reduce the signal-to-noise ratio (SNR) during imaging. Considering the confocal pinhole filtering capability (*i.e.*, 120 nm in lateral and 160 nm in axial directions), the reflected light from the subdiffractive cross-section illuminated by the central lobe can be isolated from the noises caused by the side lobe (as the dashed line illustrates in Figure 5d) and the normal paraxial focal point (as the dashed line indicates in Figure 5e). This means that only the light, of which the intensity represents the structural detail of the subdiffractive cross-section, can pass through the confocal pinhole. The super-resolution SNR is therefore increased.

Furthermore, the distance from the target surface to the microsphere center could be slightly greater or less than the microsphere radius due to the deflection of the incident light during scanning and the imperfection of the microsphere. Figure 5f shows the variations of the central lobe FWHM on the target surface with the distance (d) from a perfect microsphere bottom for various microspheres. It can be seen that all the microspheres used in this work can generate a subdiffractive central lobe (*i.e.*, illumination light spot). The minimal FWHMs of the central lobes *via* a 7.5 μm diameter FS microsphere and a 5 μm diameter PS microsphere are close to 120 nm near the microsphere bottom within a distance of 200 nm. The focusing power of the 2.5 μm diameter FS microsphere is relatively weak,

by which the FWHM of the central lobe is >170 nm. Hence, the imaging resolution using the 2.5 μm diameter FS microsphere should be the lowest. On the contrary, the 5 μm diameter FS microsphere is most suitable to focus the light into a small region (where FWHM $\approx$ 90 nm). Therefore, it would achieve the highest resolution. From the simulation results, it should be noted that the sub-diffractive central lobes exist only in the near-field within a distance of $\pm$400 nm ($\sim 2\lambda$) from the microsphere bottom.

The near-field central lobes provide sub-diffraction-limited illumination during scanning confocal imaging. Considering the refractive index of the sample, *e.g.*, AAO ($n = 1.78$ at 408 nm wavelength), the FWHM of the central lobe in the sample can be further reduced to $1/n$, where n is the refractive index of the sample. The minimal FWHM *via* a 5 μm diameter FS microsphere is therefore reduced to 50 nm in the AAO sample. We assumed the central lobe to be a normalized Gaussian distribution. The theoretical imaging resolution of the mSLCM can be identified by a 1D numerical calculation. A grating with a period of $2R$ and a duty cycle of 50% was used in the calculation. When the central lobe irradiates the grating (Figure 6a), the reflected light intensity can be expressed as

$$I = \sum_{n=-\infty}^{+\infty} \int_{(4n-1)R}^{(4n+1)R} e^{-2x^2/0.722\mathrm{FWHM}^2}\, dx \qquad (1)$$

Under the scanning imaging mode, the reflected light intensity varies with the beam moving a distance of l, which can be written as

$$I(l) = \sum_{n=-\infty}^{+\infty} \int_{(4n-1)R}^{(4n+1)R} e^{-2(x-l)^2/0.722\mathrm{FWHM}^2}\, dx \qquad (2)$$

It was assumed that the reflected light is completely collected by the mSLCM. Therefore, the reflected light intensity profile during the central lobe scanning can be plotted as Figure 6b. As can be seen, the imaging contrast of the grating is reduced with shortening the grating period. The variations of imaging contrast with the grating width R for various microspheres are plotted as Figure 6c. Considering the high sensitivity of SLCM for photons collection (where the resolvable image contrast is down to 5% according to the calculation from the SLCM specification), the calculated maximal theoretical resolutions of 2.5 μm diameter FS, 5 μm diameter FS, 7.5 μm diameter FS and 5 μm diameter PS microspheres are 46 nm, 22 nm, 35 and 36 nm, respectively, for the AAO sample. They are close to the nanostructural feature size ($\sim$25 nm) in the AAO sample. Therefore, the 25 nm imaging resolution can be achieved using the mSLCM without the effect of SPPs. For NWs, the imaging resolution using a 5 μm diameter FS microsphere is 40 nm as the ambient media is air ($n \approx 1$). Therefore, the 5 μm diameter FS mSLCM has the power to resolve 40 nm diameter Ag NWs and 50 nm diameter WO_3 NWs as shown in Figure 3. For the gold quintuplet-nanodots coated glass ($n \approx 1.5$), the imaging resolution should be around 26 nm using a 5 μm diameter FS microsphere according to the above calculation. Hence, the 25 nm separations between the nanodots can nearly be observed. It should also be noted that the subdiffractive central lobe is only located near the microsphere bottom (i.e., the contact of the microsphere and the substrate surface) and thereby the nanostructures close to the microsphere center can be imaged but the rest is blurred and distorted due to being out of central lobe focus and spherical aberration, as shown in Figure 4.

CONCLUSIONS

In this work, we presented a microsphere-coupled SLCM (mSLCM) for optical super-resolution imaging. Using a 408 nm wavelength illuminating laser, 25 nm imaging resolution ($\sim\lambda/17$) under the reflection illumination mode was demonstrated. The root of the mSLCM super-resolution imaging was due to the near-field super-resolution illumination spot focused by microspheres. When the illuminating light penetrates through a microsphere, a subdiffractive central lobe is generated near the microsphere bottom. The width and length of the central lobe along lateral and axial directions are generally shorter than $\lambda/2$ and 2λ, respectively. The sub-diffraction-limited central lobe generates a subwavelength reflecting cross-section on the target surface. Although the side lobe existing around the central one in the focusing plane and the far-field focal point in the axial direction contain the vast majority of the light energy, the pinhole of the SLCM can isolate the reflected light from the near-field subdiffractive cross-section illuminated by the central lobe and suppress the noises from the side lobe as well as far-field paraxial focal point. The pinhole filtering effect significantly increases the SNR from the subdiffractive cross-section. The structural detail of the subdiffractive cross-section is therefore captured, and the 2D target surface near the microsphere bottom can be imaged by SLCM intensity-based point scanning. A 25 nm ($\sim\lambda/17$) direct optical imaging resolution was experimentally demonstrated in this work *via* mSLCM. The present study opens up new opportunities to understand and develop microsphere-coupled scanning laser confocal nanoscopy for higher resolution imaging ($<\lambda/17$).

METHODS

AAO Sample. The AAO used in Figure 2a was fabricated by a two-step anodizing of 0.3 mm thick aluminum in sulfuric acid (0.35 mol L^{-1}) under a constant voltage of 18 V and an oxidizing temperature of 4 °C. The oxidizing times are 1 and 2 h for the first and the second steps, respectively.

Imaging Method. The microspheres were first sufficiently diluted ($<10^3$ μL^{-1}) by deionized water and then deposited onto the substrate surface by drop coating. The images were then captured after the microsphere suspension was dried, and all the microspheres were discrete on the substrate surface in a monolayer in order to avoid light interference during imaging. It should be noted that only the nanostructural features near the contact of the microsphere and substrate surface can be resolved, and the rest of the region is distorted and blurred due to being out of the central lobe focus and spherical aberration. The SLCM used in this work was an Olympus LEXT-OLS3100 fitted with 50× and 100× objective lenses (MPLAPO), of which both NAs are 0.95. The illuminating laser (wavelength = 408 ± 5 nm) is focused by the objective lens, and the reflection illumination mode without fluorescence was selected as shown in Figure 1b. The nominal lateral and axial resolutions of the SLCM are 120 nm (λ/3.4) and 160 nm (λ/2.6), respectively.

Conflict of Interest: The authors declare no competing financial interest.

REFERENCES AND NOTES

1. Durig, U.; Pohl, D. W.; Rohrer, H. Near-Field Optical-Scanning Microscopy. *J. Appl. Phys.* **1986**, *59*, 3318–3327.
2. Betzig, E.; Lewis, A.; Harootunian, A.; Isaacson, M.; Kratschmer, E. Near Field Scanning Optical Microscopy (NSOM). *Biophys. J.* **1986**, *49*, 269–279.
3. Courjon, D.; Bainier, C. Near Field Microscopy and Near Field Optics. *Rep. Prog. Phys.* **1994**, *57*, 989–1028.
4. Hsu, J. W. P. Near-Field Scanning Optical Microscopy Studies of Electronic and Photonic Materials and Devices. *Mater. Sci. Eng., R* **2001**, *33*, 1–50.
5. Pendry, J. B. Negative Refraction Makes a Perfect Lens. *Phys. Rev. Lett.* **2000**, *85*, 3966–3969.
6. Fang, N.; Lee, H.; Sun, C.; Zhang, X. Sub-Diffraction-Limited Optical Imaging with a Silver Superlens. *Science* **2005**, *308*, 534–537.
7. Zhang, X.; Liu, Z. W. Superlenses to Overcome the Diffraction Limit. *Nat. Mater.* **2008**, *7*, 435–441.
8. Smolyaninov, I. I.; Hung, Y. J.; Davis, C. C. Magnifying Superlens in the Visible Frequency Range. *Science* **2007**, *315*, 1699–1701.
9. Jacob, Z.; Alekeyev, L. V.; Narimanov, E. Optical Hyperlens: Far-Field Imaging beyond the Diffraction Limit. *Opt. Express.* **2006**, *14*, 8247–8256.
10. Liu, Z.; Lee, H.; Xiong, Y.; Sun, C.; Zhang, X. Far-Field Optical Hyperlens Magnifying Sub-Diffraction-Limited Objects. *Science* **2007**, *315*, 1686.
11. Mansfield, S. M.; Kino, G. S. Solid Immersion Microscope. *Appl. Phys. Lett.* **1990**, *57*, 2615–2616.
12. Karrai, K.; Lorenz, X.; Novotny, L. Enhanced Reflectivity Contrast in Confocal Solid Immersion Lens Microscopy. *Appl. Phys. Lett.* **2000**, *77*, 3459–3461.
13. Huang, F. M.; Zheludev, N. I. Super-Resolution without Evanescent Waves. *Nano Lett.* **2009**, *9*, 1249–1254.
14. Baumgartl, J.; Kosemeier, S.; Mazilu, M.; Rogers, E. T. F.; Zheludev, N. I.; Dholakia, K. Far Field Subwavelength Focusing Using Optical Eigenmodes. *Appl. Phys. Lett.* **2011**, *98*, 181109.
15. Rogers, E. D. F.; Savo, S.; Lindberg, J.; Roy, T.; Dennis, M. R.; Zheludev, N. I. Super-Oscillatory Optical Needle. *Appl. Phys. Lett.* **2013**, *102*, 031108.
16. Rogers, E. T. F.; Lindberg, J.; Roy, T.; Savo, S.; Chad, J. E.; Dennis, M. R.; Zheludev, N. I. A Super-Oscillatory Lens Optical Microscope for Subwavelength Imaging. *Nat. Mater.* **2012**, *11*, 432–435.
17. Lee, J. Y.; Hong, B. H.; Kim, W. Y.; Min, S. K.; Kim, Y.; Jouravlev, M. V.; Bose, R.; Kim, K. S.; Hwang, I.; Kaufman, L. J.; *et al.* Near-Field Focusing and Magnification through Self-Assembled Nanoscale Spherical Lenses. *Nature* **2009**, *460*, 498–501.
18. Mason, D. R.; Jouravlev, M. V.; Kim, K. S. Enhanced Resolution beyond the Abbe Diffraction Limit with Wavelength-Scale Solid Immersion Lenses. *Opt. Lett.* **2010**, *35*, 2007–2009.
19. Smolyaninov, I. I.; Elliott, J.; Zayats, A. V.; Davis, C. C. Far-Field Optical Microscopy with a Nanometer-Scale Resolution Based on the in-Plane Image Magnification by Surface Plasmon Polaritons. *Phys. Rev. Lett.* **2005**, *94*, 057401.
20. Smolyaninova, V. N.; Smolyaninov, I. I.; Kildishev, A. V.; Shalaev, V. M. Maxwell Fish-Eye and Eaton Lenses Emulated by Microdroplets. *Opt. Lett.* **2010**, *35*, 3396–3398.
21. Hao, X.; Liu, X.; Kuang, C. F.; Li, Y. H.; Ku, Y. L.; Zhang, H. J.; Li, H. F.; Tong, L. M. Far-Field Super-Resolution Imaging Using Near-Field Illumination by Micro-Fiber. *Appl. Phys. Lett.* **2013**, *102*, 013104.
22. Wang, Z.; Guo, W.; Li, L.; Luk'Yanchuk, B.; Khan, A.; Liu, Z.; Chen, Z.; Hong, M. Optical Virtual Imaging at 50 nm Lateral Resolution with a White-Light Nanoscope. *Nat. Commun.* **2011**, *2*, 218.
23. Chen, Z.; Taflove, A.; Backman, V. Photonic Nanojet Enhancement of Backscattering of Light by Nanoparticles: A Potential Novel Visible-Light Ultramicroscopy Technique. *Opt. Express.* **2004**, *12*, 1214–1220.
24. Li, X.; Chen, Z.; Taflove, A.; Backman, V. Optical Analysis of Nanoparticles *via* Enhanced Backscattering Facilitated by 3-D Photonic Nanojets. *Opt. Express.* **2005**, *13*, 526–533.
25. Chen, Z.; Taflove, A.; Li, X.; Backman, V. Superenhanced Backscattering of Light by Nanoparticles. *Opt. Lett.* **2006**, *31*, 196–198.
26. Heifetz, A.; Huang, K.; Sahakian, A.; Li, X.; Taflove, A.; Backman, V. Experimental Confirmation of Backscattering Enhancement Induced by a Photonic Jet. *Appl. Phys. Lett.* **2006**, *89*, 221118.
27. Yang, S.; Taflove, A.; Backman, V. Experimental Confirmation at Visible Light Wavelengths of the Backscattering Enhancement Phenomenon of the Photonic Nanojet. *Opt. Express.* **2011**, *19*, 7084–7093.
28. Li, L.; Guo, W.; Yan, Y.; Lee, S.; Wang, T. Label-Free Super-Resolution Imaging of Adenoviruses by Submerged Microsphere Optical Nanoscopy. *Light: Sci. Appl.* **2013**, *2*, e104.
29. Hao, X.; Kuang, C.; Liu, X.; Zhang, H.; Li, Y. Microsphere Based Microscope with Optical Super-Resolution Capability. *Appl. Phys. Lett.* **2011**, *99*, 203102.
30. Darafsheh, A.; Walsh, G. F.; Negro, L. D.; Astratov, V. N. Optical Super-Resolution by High-Index Liquid-Immersed Microspheres. *Appl. Phys. Lett.* **2012**, *101*, 141128.
31. Lee, S.; Li, L.; Wang, Z.; Guo, W.; Yan, Y.; Wang, T. Immersed Transparent Microsphere Magnifying Sub-Diffraction-Limited Objects. *Appl. Opt.* **2013**, *52*, 7265–7270.
32. Lee, S.; Li, L.; Ben-Aryeh, Y.; Wang, Z.; Guo, W. Overcoming the Diffraction Limit Induced by Microsphere Optical Nanoscopy. *J. Opt.* **2013**, *15*, 125710.
33. Ye, R.; Ye, Y.; Ma, H. F.; Ma, J.; Wang, B.; Yao, J.; Liu, S.; Cao, L.; Xu, H.; Zhang, J. Experimental Far-Field Imaging Properties of a ~5-μm Diameter Spherical Lens. *Opt. Lett.* **2013**, *38*, 1829–1831.
34. Guo, H.; Han, Y.; Weng, X.; Zhao, Y.; Sui, G.; Wang, Y.; Zhuang, S. Near-Field Focusing of the Dielectric Microsphere with Wavelength Scale Radius. *Opt. Express.* **2013**, *21*, 2434–2443.
35. Ben-Aryeh, Y. Superresolution Observed from Evanescent Waves Transmitted through Nano-Corrugated Metallic Films. *Appl. Phys. B: Laser Opt.* **2012**, *109*, 165–170.
36. Duan, Y.; Barbastathis, G.; Zhang, B. Classical Imaging Theory of a Microlens with Super-Resolution. *Opt. Lett.* **2013**, *38*, 2988–2990.
37. Krivitsky, L. A.; Wang, J. J.; Wang, Z.; Luk'yanchuk, B. Locomotion of Microspheres for Super-Resolution Imaging. *Sci. Rep.* **2013**, *3*, 3501.
38. Webb, R. H. Confocal Optical Microscopy. *Rep. Prog. Phys.* **1996**, *59*, 427–471.
39. Mazilu, M.; Baumgrtl, J.; Kosmeier, S.; Dholakia, K. Optical Eigenmodes: Exploiting the Quadratic Nature of the Energy Flux and of Scattering Interactions. *Opt. Express.* **2011**, *19*, 933–945.